Antibody-Guided *In Vivo* Imaging for Early Detection of Mammary Gland Tumors[1,2]

CrossMark

Laura Jeffords Moore[*], **Lopamudra Das Roy**[*,†],
Ru Zhou[*], **Priyanka Grover**[*], **Shu-ta Wu**[*],
Jennifer M. Curry[*], **Lloye M. Dillon**[*,†],
Priya M. Puri[*], **Mahboubeh Yazdanifar**[*],
Rahul Puri[†], **Pinku Mukherjee**[*,†] and **Didier Dréau**[*]

*Department of Biological Sciences, University of North Carolina at Charlotte, 9201 University City Blvd., Charlotte, NC 28223 USA; †OncoTAb, Inc., 243 Bioinformatics, 9201 University City Blvd., Charlotte, NC 28223, USA

Abstract

BACKGROUND: Earlier detection of transformed cells using target-specific imaging techniques holds great promise. We have developed TAB 004, a monoclonal antibody highly specific to a protein sequence accessible in the tumor form of MUC1 (tMUC1). We present data assessing both the specificity and sensitivity of TAB 004 *in vitro* and in genetically engineered mice *in vivo*. *METHODS:* Polyoma Middle T Antigen mice were crossed to the human MUC1.Tg mice to generate MMT mice. In MMT mice, mammary gland hyperplasia is observed between 6 and 10 weeks of age that progresses to ductal carcinoma *in situ* by 12 to 14 weeks and adenocarcinoma by 18 to 24 weeks. Approximately 40% of these mice develop metastasis to the lung and other organs with a tumor evolution that closely mimics human breast cancer progression. Tumor progression was monitored in MMT mice (from ages 8 to 22 weeks) by *in vivo* imaging following retro-orbital injections of the TAB 004 conjugated to indocyanine green (TAB-ICG). At euthanasia, mammary gland tumors and normal epithelial tissues were collected for further analyses. *RESULTS: In vivo* imaging following TAB-ICG injection permitted significantly earlier detection of tumors compared with physical examination. Furthermore, TAB-ICG administration in MMT mice enabled the detection of lung metastases while sparing recognition of normal epithelia. *CONCLUSIONS:* The data highlight the specificity and the sensitivity of the TAB 004 antibody in differentiating normal versus tumor form of MUC1 and its utility as a targeted imaging agent for early detection, tumor monitoring response, as well as potential clinical use for targeted drug delivery.

Translational Oncology (2016) 9, 295–305

Introduction

In the past decade, survival of patients with breast cancer has improved [1–3]. Routine mammograms and other screening approaches have been associated with early detection of breast cancers [4,5]. However, the repeated use of mammograms is not without risk [4], and clinical guidelines remain highly debated [4]. Chiefly, mammograms overall miss 25% of tumors and up to 50% of the tumors in late-stage diagnosis of women with extremely dense breasts [4,6–8], resulting in late stage diagnosis. It is becoming clear that cancer cells undergo specific molecular transformations long before there is a detectable change in tumor morphology. The ability to detect at these earliest stages of molecular dysregulation, before any

obvious symptoms have developed, would permit better therapeutic intervention. Thus, the concept of molecularly targeted diagnostic approaches would be very valuable.

MUC1 is a conserved transmembrane protein with an extensive extracellular domain composed of repeated glycosylated peptide motifs [9,10]. In tumor cells including breast tumors, these motifs are hypoglycosylated and the MUC1 distribution is altered [11–13]. In addition, as early as hyperplasia stages, the distribution and glycosylation of MUC1 are altered and the cell-cell organization disrupted [12,14]. As such, MUC1 is viewed as a key therapeutic target in patients with breast cancer [15,16]. In breast cancers, presence of circulatory MUC1 is associated with cancer progression and can be monitored through detection of MUC1 (CA-15-3 antigen) circulatory concentrations [17–19]. However, CA-15-3 tests rely mostly on the tumor burden and shed MUC1 and lack the specificity to identify hypoglycosylated MUC1, a hallmark of breast cancer progression. We have developed a new antibody that specifically detects altered hypoglycosylated form of MUC1 (tMUC1): TAB 004 (OncoTAb, Inc., Charlotte, NC) [20].

Breast cancer progression is uniquely modeled in the immune-competent spontaneous murine MMT model [10,21]. Derived from the PyMT model of spontaneous breast cancer and genetically engineered to express the human form of hypoglycosylated mucin-1 (tMUC1), the MMT mice develop spontaneous mammary gland tumors expressing the human form of tMUC1 [10]. In those mice, as in the parental PyMT mice, mammary gland hyperplasia is observed between 6 and 10 weeks of age that progresses to ductal carcinoma *in situ* by 12 to 14 weeks and adenocarcinoma by 18 to 24 weeks, and approximately 40% of the mice develop metastasis to the lung and other organs [10]. In MMT mice, mammary tumor evolution closely mimics human breast cancer progression. The tumors are basal in cell origin and Her-2 + subtype [10].

Here we investigated the specificity and sensitivity of TAB 004 for the early detection and monitoring of mammary tumor progression in the MMT mice. Results indicate that TAB 004 specifically immunoreacts with human tMUC1 and, when conjugated to an imaging agent, indocyanine green (ICG), allows the early detection and monitoring of mammary tumor progression and metastases by *in vivo* imaging systems.

Material and Methods

Chemical and Reagents

TAB 004 was graciously provided for the study by OncoTAb Inc. Conjugation kits to derive biotin-conjugated, horseradish peroxidase (HRP)–conjugated, and ICG-conjugated TAB 004 were obtained from Dojindo Molecular Technologies, Inc. (Rockville, MD) and used according to manufacturers' recommendations.

Generation of TAB 004 Antibody

Briefly, TAB 004 antibody (patent #US-2011-0123442, PCT/US2011/037972) is a mouse IgG1 monoclonal antibody obtained through the hybridoma approach and selected for its specific binding to extracellular repeated sequences of tumor associated MUC1 altered, i.e., hypoglycosylated MUC1 protein specifically the TAPPA sequence and the specific epitope (STAPPVHNV) [20]. The production of TAB 004 is currently conducted in batches of antibody rigorously assayed for consistent binding, stability, and purity (Supplemental Figure 1S, *A–C*; LakePharma Inc., Belmont, CA).

Cells and In Vitro Cultures

Murine cells PyMT and MMT were derived as described previously [10]. The PyMT cell line was derived from PyMT tumor, and the MMT cell line was obtained by stably expressing full-length MUC1 in PyMT cells. Both cell lines were derived in Dr. Mukherjee's laboratory originally in 1998 and stored in multiple vials in liquid nitrogen. Cells were authenticated by polymerase chain reaction for specific DNA signatures for the polyoma middle T antigen; the MMTV promoter; and, for MMT cells, the human MUC1 gene. Additionally, in MMT cells, the cell surface expression of human MUC1 was also assessed by Western blot (WB) and flow cytometry. For this study, the PyMT and MMT cells used were authenticated using the characterization methods described above within 6 to 12 months of their use. All cells used either to generate lysates or for cytometry investigations were cultured in sterile conditions in Dulbecco's modified Eagle's medium in the presence of antibiotics and antifungals supplemented with FBS and incubated at 37°C, >90% humidity, and 5% CO_2 conditions.

Orthotopic Mammary Tumor Model

MMT cells were implanted in the mammary pad of C57bl/6 6- to 8-week-old female mice, and the tumor growth was monitored using both physical examination including caliper to measure tumor growth and fluorescent monitoring as described for MMT spontaneous tumor model (see below). Controls included mice similarly implanted with PyMT cells. Furthermore, the route of injection of TAB 004 was assessed in the orthotopic model. Briefly, C57bl/6 mice implanted orthotopically with MMT tumor cells were injected 2 to 3 weeks post–tumor implantation with either saline (vehicle control) or intratumorally, intravenously, or intraperitoneally with TAB 004 conjugated with biotin, and tissues including tumor, spleen, kidneys, liver, and lungs were collected 24 hours later. Tissues were fixed and embedded in paraffin, and the presence of biotin-conjugated TAB 004 in the different tissues was assessed following incubation with streptavidin-HRP and 3,3'-diaminobenzidine (DAB). As shown in Figure 2S, in the absence of antibody, no HRP activity was detected. HRP activity associated with the HRP-conjugated TAB 004 antibody was faintly, highly, and strongly detected in tumor following intratumoral, intravenous, and intraperitoneal injections, respectively. With the exception of the spleen, in animals administered biotin-conjugated TAB 004 intravenously, no other organ exhibited an HRP activity associated with the HRP-conjugated TAB 004 antibody.

Specificity and Sensitivity of TAB 004 Antibody

The presence of altered MUC-1 was also determined by flow cytometry and WB on PyMT and MMT murine cells using TAB 004. Briefly, for flow cytometry analyses, cells were grown in culture conditions described above; detached from vessels; and, following a blocking step incubated with TAB 004 antibody (30 minutes) and after a secondary antibody stain (15 minutes), run on a Fortessa flow cytometer (BD-Biosciences, San Jose, CA). Raw data were further analyzed using FlowJo Software (Ashland, OR). Data are presented as histogram with information on mean fluorescence intensity and percentage of positive cells along with controls. Additionally, PyMT and MMT cell lysates and MMT tumor mass lysates were assessed by WBs. Briefly, lysates were obtained from cell cultured as described above and from MMT tumors through incubation with lysis buffer as described previously [22,23]. Cell lysates were stored at –80°C until use. Following electrophoresis in reducing conditions and transfer to

polyvinylidene difluoride membranes, the presence of altered tMUC1 was determined using TAB 004 antibody (overnight, 4°C) and revealed using ECL reagent (ThermoFisher Scientific, Waltham, MA). β-Actin was used as the loading control.

Monitoring Mammary Tumor Growth in the MMT Spontaneous Murine Model

All mice were monitored and followed in accordance with the University of North Carolina at Charlotte Institutional Animal Care and Use Committee–approved protocol. MMT mice were genetically derived from PyMT mice (C57BL/6 background) that spontaneously develop mammary tumors and specifically express MUC1 [10]. Spontaneous tumor progression follows a similar time line in PyMT and MMT female mice. From puberty (6-8 weeks old) onward, mammary tissues expressing the polyoma middle T antigen driven by the MMTV promoter mimic all the steps of breast cancer progression in humans including hyperplasia, ductal carcinoma in situ, invasive carcinoma, and metastasis [10] at any given time from 8 up to 22 to 24 weeks of age. Furthermore, multiple tumor masses at different stages are present in this spontaneous model of breast cancer progression. This murine model is aggressive as most animals (>95%) develop multiple mammary tumor lesions which are usually palpable by 14 to 16 weeks of age [10]. The main difference in tumor progression between PyMT and MMT mice is the expression of murine and human MUC1 glycoprotein, respectively [10].

Here, MMT mice were monitored in vivo for tumor progression using the in vivo imaging system (IVIS; Perkin Elmer, Waltham, MA). Both C57Bl/6 and PyMT mice were used as controls. In vivo monitoring was conducted according to manufacturer's recommendations, following injections of TAB 004 conjugated with the fluorophore indocyanine green (TAB-ICG). ICG has been shown to have no significant side effects and is currently FDA-approved for multiple procedures including angiography [24]. Before each imaging sequence, TAB-ICG in sterile saline was administered retro-orbitally or intraperitoneally to mice, and imaging was conducted 0.5, 4, 24, and 48 hours postinjection. Animals were injected and imaged every 2 weeks for tumor progression. Tumor fluorescence was analyzed using the Life Science Software Suite (Perkin Elmer), and region of interest was defined at tumor location. In parallel, the presence of tumor masses was assessed by palpation and recorded. Additionally, after mouse euthanasia, further analyses of tumors (T) and specific organs including mammary pads (MP), liver (Li), lungs (Lu), spleen (S), and kidneys (K) were conducted ex vivo using the IVIS system and by histology and immunohistochemistry (IHC; see below).

MMT spontaneous mammary tumor growth was also monitored over time for gross pathology, cellular morphology, and the presence of specific markers including tMUC1 using IHC with TAB 004 antibody (see below).

Monitoring Mammary Tumor Lung Metastases in the MMT Spontaneous Murine Model

In the PyMT and MMT mouse models, early metastases, which occur in the lungs, is masked in vivo by the fluorescence emitted by larger tumors. Therefore, ex vivo analyses of organs isolated posteuthanasia were conducted using the IVIS system. The fluorescence signal (expressed as fluorescence units) was normalized to the background fluorescence generated by each organ specifically the lung, liver, spleen, and brain from control MMT mice (i.e., MMT mice not injected with TAB-ICG). Additionally, the presence of lung metastases was determined following fixation, embedding,

and sectioning of the lungs of MMT mice. Briefly, lungs from animals 16 weeks or older were collected 24 hours postinjections and embedded in paraffin. Five- to six-micrometer–thick sections were obtained, stained with hematoxylin and eosin (H&E), and examined for the presence of metastases.

Detection of tMUC1 by IHC

The expression of human altered MUC1 (tMUC1) was determined in murine tumors using TAB 004. Murine tumors from PyMT and MMT mice and normal mammary gland from C57bl/6 mice were collected. Samples were fixed in buffered formalin and embedded in paraffin, and 5- to 6-µm–thick sections were obtained. In addition to H&E staining, murine samples were assessed for expression of tMUC1 using TAB 004 antibody. Briefly, either unconjugated TAB 004 antibody followed with a second step detection with an anti-mouse HRP-conjugated secondary antibody or the TAB 004-HRP conjugated was used. The staining procedure includes a blocking step, incubation with primary antibody (overnight, 4°C) and secondary antibody (1 hour), or incubation with primary antibody conjugated with HRP (overnight, 4°C). In both approaches, the presence of TAB 004 antibody was revealed using DAB with a hematoxylin counterstain followed by mounting the tissue slides. Tissue slides were then assessed by light microscopy, and microphotographs were taken using a DP70 camera and the Olympus Software Suite (Olympus, Waltham, MA).

Statistical Analyses

The linearity associating TAB 004 dose with the detection of tMUC1 was assessed by linear regression. The difference between methods in early detection time was determined by unpaired t test. The detection of lung metastases was assessed by one-way ANOVA followed with post hoc tests with a priori significance sets at $P < .05$.

Results

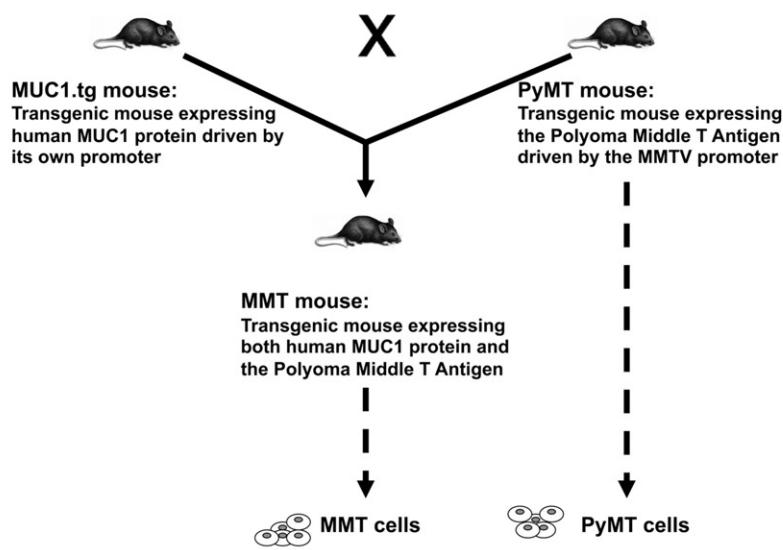### The MMT Murine Model Mimics Human Breast Cancer Progression

The MMT mouse model has been described previously [10]. Briefly, as schematized in Figure 1A, this spontaneous model of mammary tumor progression was developed through the generation of double transgenic mice by crossing of mice expressing human MUC1 gene [25] and mice expressing the polyoma middle T antigen under the MMTV promoter [26]. PyMT and MMT tumor cell lines were also developed (Figure 1A). Over time, MMT tumors mimic the stages and cellular morphology of human breast cancer progression (Figure 1B). Furthermore, the biomarker tumor profiles indicate a decrease in both estrogen receptors (ERs) and progesterone receptors (PRs), increase in Neu and Cyclin D1, and decrease in integrin β as tumor progresses mimicking the ER⁻PR⁻Neu⁺ human disease [27]. In addition, tMUC1 expression detected by TAB 004 increases as tumors progress (Figure 1B), which makes this model ideal for our studies. Importantly, TAB 004 does not recognize normal mammary epithelial tissue from non–tumor-bearing control mice (Figure 1B). The monoclonal antibody TAB 004 recognizes the hypoglycosylated tandem repeat epitope within the STAPPVHNV sequence of human MUC1 [20].

TAB 004 Specifically Recognizes tMUC1 In Situ by IHC, In Vitro by Flow Cytometry, and In Vivo Following Orthotopic Implantation of MMT Cells
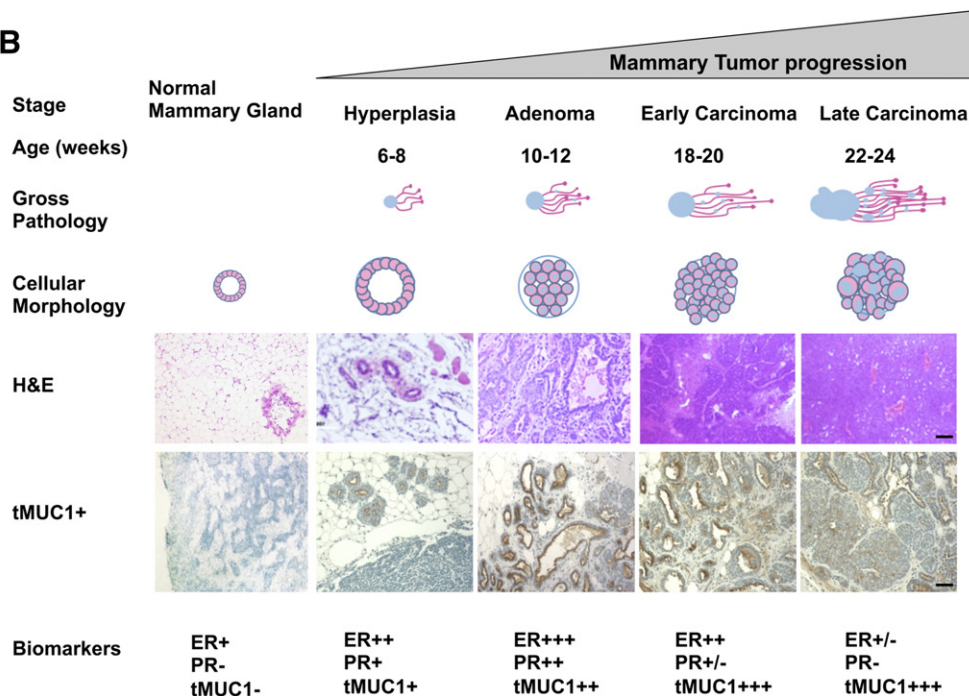
PyMT and MMT cell lines were tested for tMUC1 expression in vitro and in vivo. Compared with PyMT cells, MMT cells expressed

Figure 1. (A) Human MUC1 expressing mammary tumor (MMT) transgenic mouse model and associated PyMT and MMT tumor cells. Briefly, the spontaneous MMT mammary tumor model was generated through the cross of MUC1.tg mice [C57BL/6-Tg(MUC1)79.24Gend/J mice] [25] with PyMT mice [FVB/N-Tg(MMTV-PyVT)634Mul/J mice] [26]. The resulting dual transgenic female mice spontaneously develop mammary tumors that express human MUC1. Additionally, associated PyMT and MMT cell lines have been developed that are transgenic for the polyoma middle T antigen and for both the polyoma middle T antigen and human MUC1, respectively. (B) Mammary tumor growth in the MMT transgenic mouse model mimics human breast cancer progression. Briefly, in the spontaneous MMT mammary tumor model, the stages of hyperplasia, adenoma, and early and late carcinoma are identified at 6 to 8, 10 to 12, 18 to 20, and 22 to 24 weeks of age, respectively. Each stage is associated with gross pathology and cellular morphology similar to those observed in human breast cancer progression as indicated by visual observation and H&E staining. Moreover, expressions of biomarkers including ERs and PRs decreased, whereas tMUC1 expression (detected using TAB 004) increased, with mammary tumor progression as determined using specific antibodies and IHC techniques (scale bar = 200 μm). Normal C57Bl/6 mammary gland is also displayed (left) and shows no staining with TAB 004.

significantly higher levels of tMUC1 as determined by TAB 004-Cy7 staining and flow cytometry (Figure 2, A and B). Additionally, IHC staining with TAB 004-HRP confirmed that TAB 004 only binds to the MMT tumors but not to the PyMT tumors, further indicating specificity to the human form of tMUC1 (Figure 2, C and D). To determine if TAB 004 specifically localizes to the MMT tumor when

injected *in vivo*, TAB-ICG was injected (retro-orbitally) into PyMT and MMT tumor-bearing mice, and tumor progression was successfully imaged in MMT mice over time using the IVIS system (Figure 2, *E* and *F*). Tumor volume was monitored by caliper measurements (Figure 2, *G* and *H*). Although both tumors grew at a similar rate, TAB-ICG only localized to the MMT but not in the PyMT tumors, and accumulation of TAB-ICG increased with tumor size (Figure 2, *E* and *F*).

Next, we determined the expression of tMUC1 in the spontaneously arising tumors dissected from the PyMT and MMT mice. By WB analysis, TAB 004 showed immunoreactivity with the tumor lysates from MMT but not from PyMT tumors (Figure 2*I*). Lysate from the MMT cell line was used as the positive control, and β-actin served as the loading control. By IHC, TAB 004 stained the MMT tumors but did not stain normal mammary epithelia or PyMT tumors (Figure 2*J*). Taken together, TAB 004 showed high specificity to human tMUC1 and did not bind to normal or mouse Muc1.

Monitoring of Mammary Tumor Progression Is Dependent on the Dose of TAB 004 Administered in the MMT Mice

The dose of TAB-ICG injected to monitor the presence of tumor mass within the MMT spontaneous mammary tumor model was assessed for doses ranging from 12.5 to 100 μg (Figure 3). As expected, regardless of the dose, the tumor fluorescent signal peaked at ~24 hours and decreased thereafter, as shown in the representative IVIS images taken over time (Figure 3*A*). When compared with the number of palpable tumors, the number of fluorescent tumors in MMT mice (8-22 weeks old) with at least one tumor mass 24 hours postinjection of TAB-ICG varied depending on the dose of TAB-ICG administered (Figure 3*B*). Indeed, whereas detection following injections of 12.5 μg or 25 μg of TAB-ICG was high, injections of 50 μg or 100 μg of TAB-ICG were associated with lower tumor mass detection (Figure 3*B*). Furthermore, analyses limited to mice with two or more tumors (11-22 weeks old) demonstrated that the fluorescent detection was correlated with the amount of
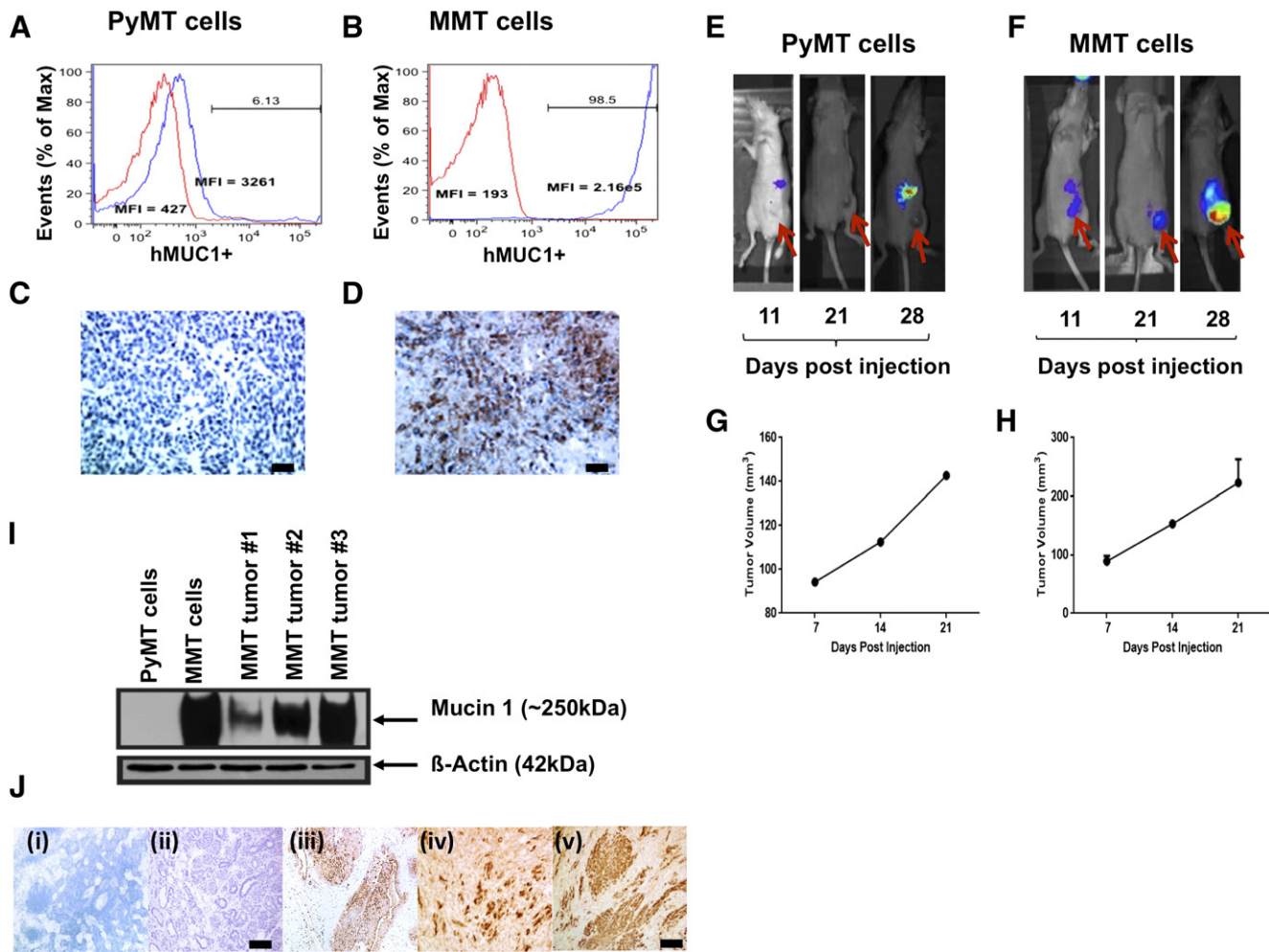
Figure 2. TAB 004 detects tMUC1 in MMT cells and allows the monitoring over time of MMT orthotopic tumor growth *in vivo*. TAB 004 detected tMUC1 in MMT cells (B) but not in PyMT cells (A) by flow cytometry and IHC (C and D), respectively (scale bar = 100 μm). When orthotopically implanted in C57Bl/6 mice, PyMT and MMT tumors grew over time (as determined by caliper measurements) (G and H) and could be monitored using ICG-conjugated TAB 004 but only for MMT tumors (E and F). By WB, HRP-conjugated TAB 004 detected human tMUC1 in lysates from MMT cells as well as in lysates from tumors collected following orthotopic implantation of MMT tumor cells but not in lysates from PyMT cells (I). Furthermore, IHC analyses (J) of normal mammary gland [C57bl/6 (i), PyMT (ii) and MMT (iii, iv, v)] using HRP-conjugated TAB 004 detected human tMUC1 (brown stain) only in MMT tumors (scale bar = 150 μm).
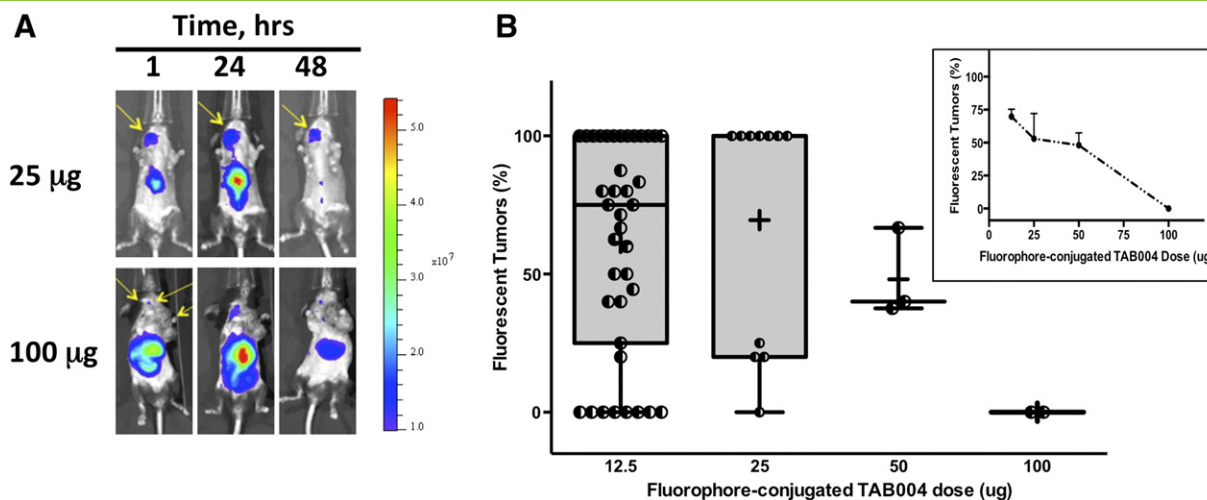
Figure 3. *In vivo* detection of mammary tumor masses in the MMT mice following TAB-ICG injection is dose-dependent. MMT mice (8-22 weeks old) with palpable tumors were repeatedly injected with ICG-conjugated TAB 004 (12.5, 25, 50, or 100 µg in sterile saline) and monitored for fluorescence using the IVIS system. (A) Representative IVIS imaging of MMT mice injected with 25 µg (top) and 100 µg (bottom) of ICG-conjugated TAB 004 taken 1, 24, and 48 hours postinjection. The fluorescent scale [from low (blue) to high (red)] indicates the presence of fluorescence with varying intensity at different location with the mice monitored. (B) Tumor mass fluorescent detection (% of palpable tumors) in MMT mice with at least one tumor mass 24 hours postinjection of ICG-conjugated TAB 004. As shown, the injection of 12.5 and 25 µg of ICG-conjugated TAB 004 was associated with improved tumor detection compared with 50 and 100 µg. Furthermore, when only mice with two or more tumors were analyzed (B, inset), the detection increased with decreasing amount of ICG-conjugated TAB 004 injected: from 0% to 75% for 100 and 12.5 µg, respectively ($r^2 = 0.96$, $P = .019$).

TAB-ICG injected (Figure 3B, insert). When the amount of TAB-ICG injected decreased, the detection using fluorescence increased: from 0% to 75% for 100 µg and 12.5 µg, respectively ($r^2 = 0.96$, $P = .019$). Thus, all subsequent studies were conducted with 12.5 µg of TAB-ICG.

Administration of TAB-ICG Enables Specific and Overtime Monitoring of tMUC1-Positive Tumors in the MMT Mice

The MMT mouse model uniquely permits the investigation of spontaneous tumor progression in an immunocompetent mouse model [10]. In this model, tumor progression leads to multiple tumor masses heterogeneous for both size and stages [10]. Nevertheless, the MMT model closely mimics human breast cancer progression [10,27]. Here, MMT and PyMT mice at 16 weeks of age bearing multiple palpable tumors were injected with TAB-ICG. The presence of TAB-ICG was monitored *in vivo* by IVIS. As shown in Figure 4A, TAB-ICG detected multiple palpable tumor masses in MMT mice but did not accumulate in any of the PyMT tumors (Figure 4A). The nonspecific fluorescence around the liver of the mice was attributed to tissue autofluorescence.

Injections of 12.5 µg of TAB-ICG allowed the overtime monitoring of mammary tumor progression in MMT mice (10, 14, 17, and 21 weeks of age) as indicated by representative IVIS images shown in Figure 4B. As indicated by the yellow asterisk in the 10-week-old MMT mice, we detected the tumor by flourescence, but there were no palpable tumors at that time. As mice aged to 14 weeks, several of those tumors that were nonpalpable became palpable as indicated by the yellow arrows. At later ages (weeks 17 and 21), the yellow arrows indicate palpable tumors with accumulation of the TAB-ICG. Whereas tumor detection by palpation and fluorescence was similar in 13-week-old and older MMT mice, tumor detection following injection of TAB-ICG was significantly increased compared with palpation in MMT mice 12 weeks of age or younger

(Figure 4C). Moreover, comparison of physical examination (i.e., palpation) and TAB 004 fluorescence indicates that primary tumors were detected significantly earlier (~ 3.4 weeks earlier) by fluorescence monitoring than by physical examination (9.4 ± 0.7 weeks of age vs 12.8 ± 0.4 weeks of age, $n = 9$, $P = .0016$, Figure 4D). Thus, TAB-ICG has the ability to detect early stages when normal MUC1 is undergoing the molecular transformation to tMUC1 much before any obvious palpable tumors appear.

Administration of TAB-ICG Enables Monitoring of tMUC1-Positive Tumors Demonstrated by Ex Vivo Assessment of Tumors Dissected from MMT Mice

To further ascertain the potential of TAB-ICG for detection of mammary tumor masses at early onset, *ex vivo* analyses were conducted. An 18-week-old MMT mouse was injected with TAB-ICG and imaged. Figure 5A shows high fluorescent signal corresponding to a large tumor. When dissected and imaged *ex vivo*, as expected, a very strong fluorescent signal was seen corresponding to the largest tumor mass, but weak fluorescent signal was also noted in the rest of the mammary fat pads (Figure 5B), indicating that these mammary glands were not normal but had transformed to express low levels of tMUC1. Thus, when mammary fat pads from 8- to 10-week-old MMT mice were assessed following TAB-ICG injection, we once again detected low fluorescent signal in some of the mammary fat pads (Figure 5C) indicating the presence of tMUC1 at very early stages of cancer progression. H&E staining confirmed and highlighted the presence of hyperplasia in those fluorescing mammary fat pads (Figure 5E (ii)), whereas the nonfluorescing mammary fat pad was composed mostly of normal tissue (Figure 5E (i)). *Ex vivo* imaging following TAB-ICG administration of tumors and mammary fat pad dissected from 18-week-old MMT mice bearing multiple tumors revealed that the amount of fluorescent signal distinguishes between tumor masses and hyperplastic
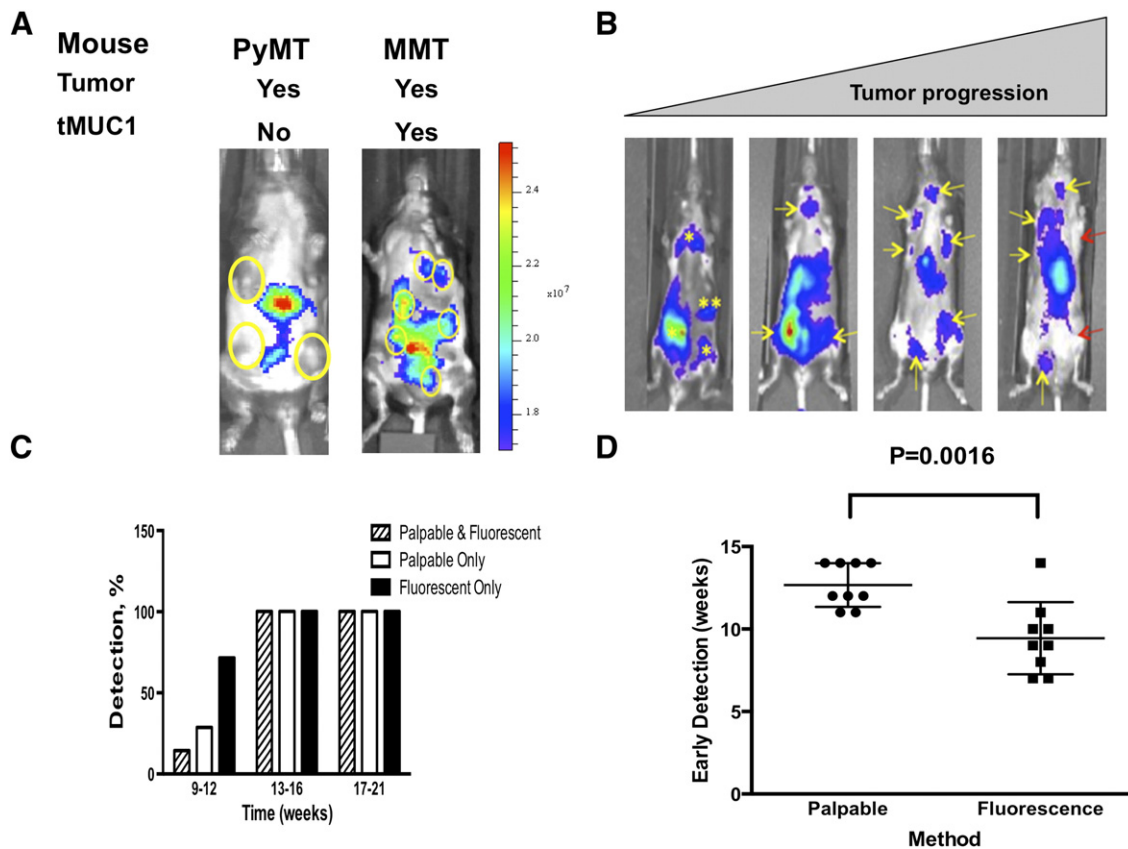
Figure 4. Early detection of primary mammary tumors in the MMT mice following TBA-ICG injection. (A) ICG-conjugated TAB 004 detected tMUC1+ tumors in MMT mice only but not in PyMT mice, where tumors were not fluorescent (only nonspecific liver fluorescence was observed). (B) Representative IVIS images of tumor masses detected in MMT mice 10, 14, 17, and 21 weeks of age. The presence of tumor mass was monitored over time in MMT mice aged 9 to 23 weeks. Both physical examination (palpation) and fluorescence monitoring using the IVIS system 24 hours postinjection of ICG-TAB 004 were collected over time. Yellow asterisks and yellow arrows indicate the presence of nonpalpable and palpable tumors, respectively, whereas red arrows note the presence of nonfluorescent palpable tumor mass essentially in older mice. (C) Whereas tumor detection by palpation and fluorescence was similar in 13-week-old and older MMT mice, tumor detection following injection of ICG-conjugated TAB 004 associated with IVIS system was increased compared with palpation in MMT mice 12 weeks old and younger. (D) Early detection indicates that primary tumors are detected significantly earlier by fluorescence monitoring than by physical examination (9.4 ± 0.7 weeks of age vs 12.8 ± 0.4 weeks of age, $n = 9$, $P = .0016$).

mammary fat pads (Figure 5D). H&E staining confirmed the extensive presence of tumor in the strongly fluorescing tumor in the 18-week-old MMT mice (Figure 5F).

Administration of TAB-ICG Allows Monitoring of tMUC1-Positive Lung Metastases Demonstrated by Ex Vivo Assessment of Fluorescent Signal in the Lungs of MMT Mice

Whether TAB 004 could detect the presence of metastases in the MMT mice was assessed *ex vivo* following *in vivo* administration of TAB-ICG. The fluorescent signal in several organs dissected from MMT mice at various ages (<16, 16-20, and >20 weeks of age) was determined using the IVIS system. No increase in fluorescence was observed in the liver, spleens, and brain of MMT mice versus normal C57BL/6 organs (data not shown). However, fluorescent signal in the lungs was significantly higher than control mouse lung, and the signal exponentially increased with the age of MMT mice (Figure 6A) [$1.71 \times 10^6 \pm 0.11 \times 10^6$, $2.21 \times 10^6 \pm 0.08 \times 10^6$, and $2.10 \times 10^6 \pm 0.05 \times 10^6$ for 8- to 11- ($n = 7$), 16- to 18- ($n = 6$), and 19- to 22- ($n = 7$) week-old MMT mice, respectively, $P < .05$]. This increase in fluorescent signal with age suggests micrometastasis in the lungs. Indeed, as in

the PyMT model, MMT mice develop metastases mainly in the lungs [10]. The presence of micrometastases was confirmed in these MMT mice following H&E staining of the lung (Figure 6B). Representative H&E shows clear lesion in the MMT lung [Figure 6B (ii)] versus no lesion in the control lung [Figure 6B (i)].

Discussion

We have demonstrated the specificity and sensitivity of TAB 004, an antibody against the hypoglycosylated form of human MUC1 (tMUC1). TAB 004 conjugated to indocyanine green (TAB-ICG) enables the *in vivo* monitoring of primary mammary tumor progression and metastasis in the MMT mice. The results highlight the early detection of neoplastic transformation as well as detect micrometastases in the lungs.

In contrast to PyMT mice, MMT mice have been genetically engineered to express human tMUC1, whereas the former express the murine form of hypoglycosylated Muc1 [10]. Those models, although significantly more aggressive than generally observed in human breast cancer progression, appropriately mimic the cancer progression from hyperplasia to adenocarcinoma and metastasis in an
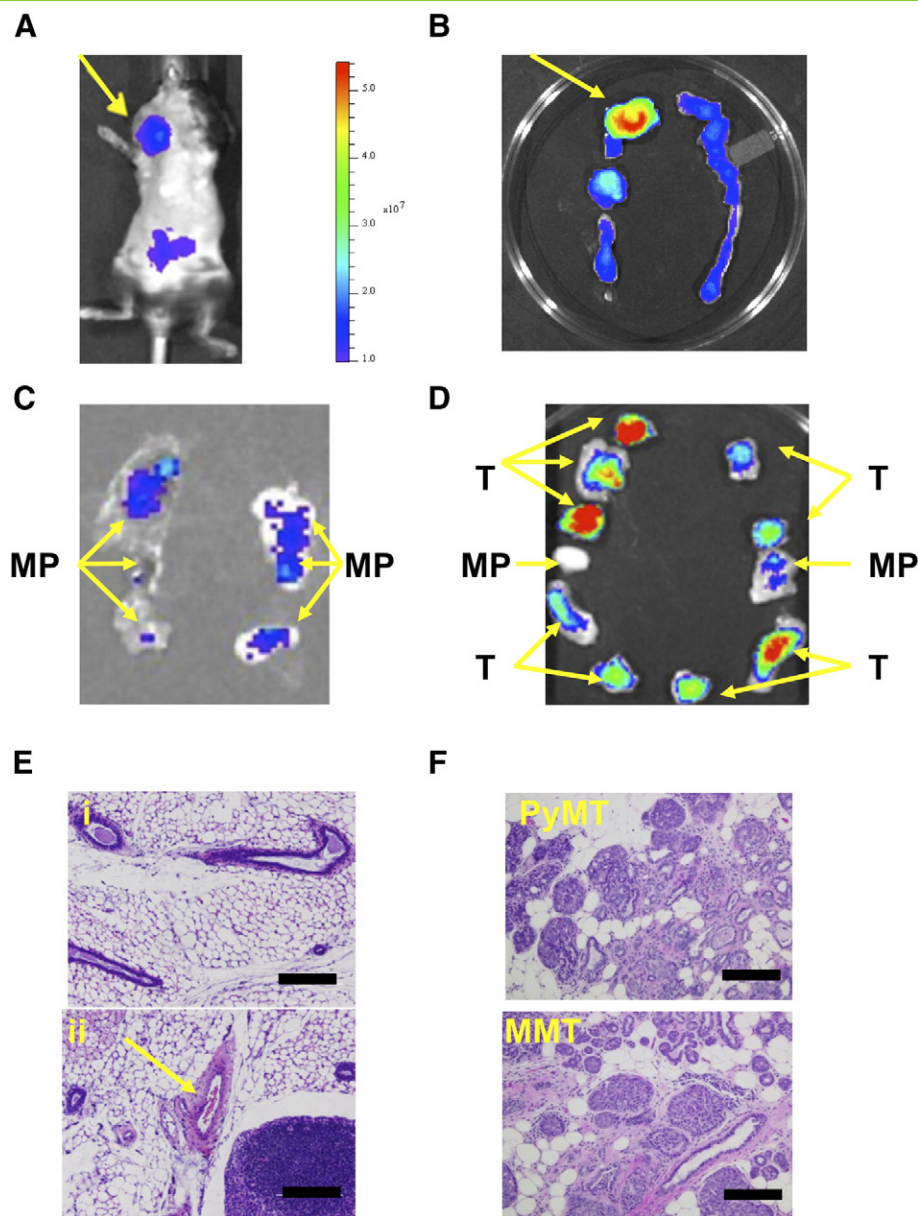
Figure 5. *Ex vivo* assessment of mammary gland tumors from MMT mice post TAB-ICG injection. Representative mouse assessed for fluorescence using IVIS system following injection of 12.5 μg of TAB 004 conjugated with ICG *in vivo* (A) and the corresponding *ex vivo* posteuthanasia mammary fat pads assessed using the same system (B). Entire mammary ridges (left and right) isolated from a 10-week-old (C) and an 18-week-old (D) MMT mouse are displayed, and the presence within the mammary pad (MP) of tumor mass (T) is noted. Furthermore, when assessed following H&E staining (scale bar = 100 μm), MP from the 10-week-old mouse presented mostly normal mammary tissues [E (i)]. However, even that early, hyperplasia was observed in a few areas of the MP [arrow, E (ii)]. In older mice (~18 weeks old), whether PyMT or MMT, the presence of tumor was extensive (F).

immunocompetent environment [10] and thus are appropriate models to investigate *in vivo* tumor detection.

TAB 004 specifically targets the transformed MUC1 protein with minimal immunoreactivity with the normal MUC1. This increased specificity of TAB 004 to tMUC1 expressed in the spontaneously arising mammary gland tumors in MMT mice is a novel finding and may allow earlier diagnosis of breast tumors. The specificity of TAB 004 was further demonstrated in MMT cell lines by IHC, WB, and flow cytometry. Extensive clinical research indicates that there are several molecular classifications of breast tumors based upon the expression of specific receptors (ER, PR, Her2/neu) and the cell origin (basal versus luminal). These subtypes are associated with

significant differences in patients' survival [28–30]. For instance, triple-negative breast cancers are more aggressive and difficult to treat. Those observations led to the generation of multiparameter tests (e.g., Oncotype DX, 21-gene recurrence score) to support therapeutic decision [31,32]. Although those tests have proven beneficial especially in determining specific treatment courses for a given tumor type [33,34], the tests are not useful for early diagnosis. The clinical use of TAB 004 may be in the space of aiding diagnosis early and accurately especially given that mammograms fail in women with dense breast 50% of the time and overall misses 25% of the tumors. Furthermore, mammograms have high false-positive rates as > 80% of biopsies post suspicious mammograms turn out to be benign. Indeed,
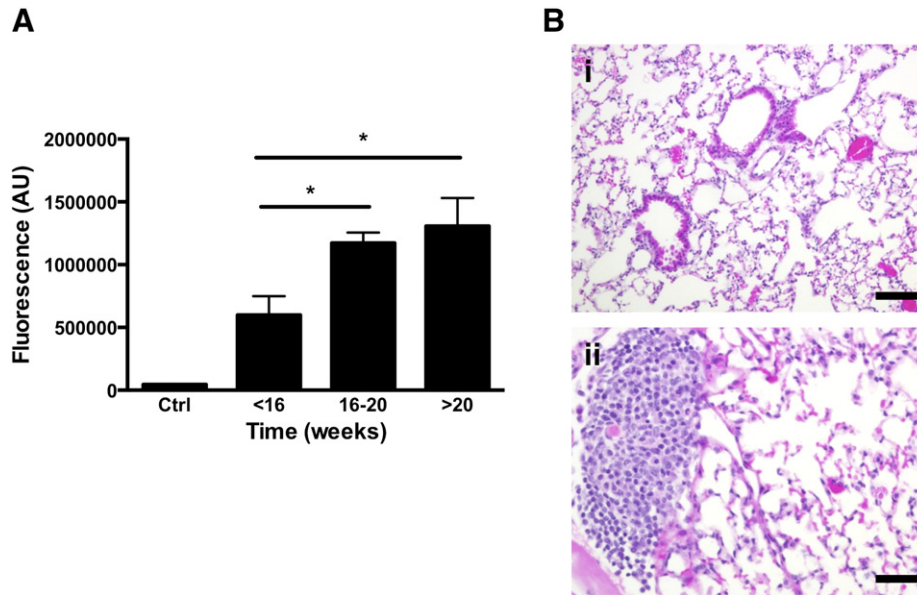
Figure 6. Detection of lung metastases in the MMT mice post TAB-ICG injection. (A) The presence of fluorescence [expressed as arbitrary unit (AU)] associated with the injection of ICG-conjugated TAB 004 was measured *ex vivo* on isolated lungs posteuthanasia using the IVIS system. Compared to control (Ctrl) lungs (lungs isolated from a noninjected MMT mouse), detected fluorescence increased with age in MMT mice [$5.99 \times 10^6 \pm 1.5 \times 10^6$, $11.73 \times 10^6 \pm 0.8 \times 10^6$, and $13.1 \times 10^6 \pm 2.23 \times 10^6$ for MMT mice <16 ($n = 7$), 16-20 ($n = 6$), and >20 ($n = 7$) weeks old, respectively; $*P < .05$]. (B) Normal lung (i) and micrometastasis (ii) in the lungs of a 16- to 17-week-old MMT female mouse stained with H&E (scale bar = 100 μm).

using a panel of 440 patient breast cancer tissue arrays, we determined that 95% of BCs express tMUC1, as detected by TAB 004 staining and IHC, regardless of the tumor subtype and density of the breast tissue (manuscript in preparation).

Although most approaches (physical, imaging, blood tests, and combination thereof) diagnose with significant accuracy the presence of advanced breast cancer, the earlier stages remain much more difficult to detect reliably [4,7,35,36]. Indeed, for those early stages including atypical hyperplasia and ductal carcinoma *in situ*, mammographic examination is associated with a high false-positive rate [6]. Similarly, the determination of circulatory CEA and or CA-15-3 antigen lacks the specificity and sensitivity in individuals with early disease, although they may be of benefit in monitoring metastasis and disease recurrence [37]. Multiple studies have demonstrated improved detection when using ultrasounds and magnetic resonance imaging (MRI) [7,38], although those approaches are mostly used to further assess suspicious mass abnormalities detected during mammography [4,38] as opposed to screening. The numbers of false-positive and to a lesser extent of false-negative cases highlight the potential of molecularly targeted imaging, especially to detect early stages of the disease and possibly micrometastasis.

Moreover, as tMUC1 is present in multiple epithelial cancers including colon carcinoma, ovarian cancer, and pancreatic cancer, TAB 004 may serve as a detecting and monitoring tool for multiple cancers. Already, preclinical and clinical observations have demonstrated the specificity of TAB 004 antibody toward tMUC1 antigen in pancreatic cancer [20].

In vivo, TAB-ICG detected primary tumors generally before they were palpable in the MMT model. The early detection of nonpalpable tumors by TAB-ICG including hyperplasia forms proof of principle of the potential use of this antibody in the clinic in conjunction with other imaging modalities. For example,

conjugated with radioactive imaging agents, TAB 004 could greatly improve the reliability of early breast cancer diagnosis when used in conjunction with computed tomography or MRI [39–43].

Interestingly, *ex vivo* imaging and H&E staining provide evidence that TAB-ICG enabled detection of lung metastases as early as 16 weeks of age in MMT mice (Figure 6). Thus, we suggest that TAB 004 conjugated to radioactive material such as technetium (99m) along with MRI and computed tomography scan may provide improved monitoring of the development of distant metastases in patients with breast cancer.

Clinically, although early detection is the key in breast cancer treatment, standard mammography generates a high number of false negatives, especially in women with dense breasts [4,6,7,44–46]. For those patients, additional examinations and imaging such as ultrasounds and MRI may be conducted. Mammography also generates false positive and biopsies, which in many cases are unwarranted [4,47]. Overall, two-dimensional mammograms have been deemed of limited use in individuals with dense breast tissues (40% of the women) [6–8] because for those patients, the mammograms are often difficult to interpret [44,48].

In summary, our investigations demonstrate the specificity of TAB 004 antibody against hypoglycosylated human MUC1 and its potential in early detection of transformed mammary epithelial cells and micrometastasis. Based on this proof of principle, we suggest that TAB 004 conjugated with contrasting agents or radioisotopes used in current clinical imaging protocols will allow both early and accurate detection and monitoring of breast cancer, even in women with dense breast tissue. We further propose that because tMUC1 is present in most epithelium-derived cancers, TAB 004 likely may be beneficial in the detection and monitoring of multiple cancers.

Supplementary data to this article can be found online at http://dx.doi.org/10.1016/j.tranon.2016.05.001.

References

[1] Campone M, Valo I, Jezequel P, Moreau M, Boissard A, Campion L, Loussouarn D, Verriele V, Coqueret O, and Guette C (2015). Prediction of recurrence and survival for triple-negative breast cancer by a protein signature in tissue samples. *Mol Cell Proteomics* **14**, 2936–2946

[2] Ward EM, DeSantis CE, Lin CC, Kramer JL, Jemal A, Kohler B, Brawley OW, and Gansler T (2015). Cancer statistics: breast cancer in situ. *CA Cancer J Clin* **65**, 481–495

[3] DeSantis C, Ma J, Bryan L, and Jemal A (2014). Breast cancer statistics, 2013. *CA Cancer J Clin* **64**, 52–62.

[4] Oeffinger KC, Fontham ET, Etzioni R, Herzig A, Michaelson JS, Shih YT, Walter LC, Church TR, Flowers CR, and LaMonte SJ, et al (2015). Breast cancer screening for women at average risk: 2015 guideline update from the American Cancer Society. *JAMA* **314**, 1599–1614.

[5] Gilbert FJ, Tucker L, Gillan MG, Willsher P, Cooke J, Duncan KA, Michell MJ, Dobson HM, Lim YY, and Purushothaman H, et al (2015). The TOMMY trial: a comparison of TOMosynthesis with digital MammographY in the UK NHS Breast Screening Programme—a multicentre retrospective reading study comparing the diagnostic performance of digital breast tomosynthesis and digital mammography with digital mammography alone. *Health Technol Assess* **19**, 1–136 [i-xxv].

[6] Kerlikowske K, Zhu W, Tosteson AN, Sprague BL, Tice JA, Lehman CD, and Miglioretti DL (2015). Identifying women with dense breasts at high risk for interval cancer: a cohort study. *Ann Intern Med* **162**, 673–681.

[7] Scheel JR, Lee JM, Sprague BL, Lee CI, and Lehman CD (2015). Screening ultrasound as an adjunct to mammography in women with mammographically dense breasts. *Am J Obstet Gynecol* **212**, 9–17.

[8] Moshina N, Ursin G, Hoff SR, Akslen LA, Roman M, Sebuodegard S, and Hofvind S (2015). Mammographic density and histopathologic characteristics of screen-detected tumors in the Norwegian Breast Cancer Screening Program. *Acta Radiol Open* **4**. http://dx.doi.org/10.1177/2058460115604340.

[9] Beatson RE, Taylor-Papadimitriou J, and Burchell JM (2010). MUC1 immunotherapy. *Immunotherapy* **2**, 305–327.

[10] Mukherjee P, Madsen CS, Ginardi AR, Tinder TL, Jacobs F, Parker J, Agrawal B, Longenecker BM, and Gendler SJ (2003). Mucin 1-specific immunotherapy in a mouse model of spontaneous breast cancer. *J Immunother* **26**, 47–62.

[11] Ideo H, Hinoda Y, Sakai K, Hoshi I, Yamamoto S, Oka M, Maeda K, Maeda N, Hazama S, and Amano J, et al (2015). Expression of mucin 1 possessing a 3'-sulfated core1 in recurrent and metastatic breast cancer. *Int J Cancer* **137**, 1652–1660.

[12] Siroy A, Abdul-Karim FW, Miedler J, Fong N, Fu P, Gilmore H, and Baar J (2013). MUC1 is expressed at high frequency in early-stage basal-like triple-negative breast cancer. *Hum Pathol* **44**, 2159–2166.

[13] Lavrsen K, Madsen CB, Rasch MG, Woetmann A, Odum N, Mandel U, Clausen H, Pedersen AE, and Wandall HH (2013). Aberrantly glycosylated MUC1 is expressed on the surface of breast cancer cells and a target for antibody-dependent cell-mediated cytotoxicity. *Glycoconj J* **30**, 227–236.

[14] Mommers EC, Leonhart AM, von Mensdorff-Pouilly S, Schol DJ, Hilgers J, Meijer CJ, Baak JP, and van Diest PJ (1999). Aberrant expression of MUC1 mucin in ductal hyperplasia and ductal carcinoma In situ of the breast. *Int J Cancer* **84**, 466–469.

[15] Alam M, Rajabi H, Ahmad R, Jin C, and Kufe D (2014). Targeting the MUC1-C oncoprotein inhibits self-renewal capacity of breast cancer cells. *Oncotarget* **5**, 2622–2634.

[16] Raina D, Agarwal P, Lee J, Bharti A, McKnight CJ, Sharma P, Kharbanda S, and Kufe D (2015). Characterization of the MUC1-C cytoplasmic domain as a cancer target. *PLoS One* **10**, e0135156. http://dx.doi.org/10.1371/journal.pone.0135156.

[17] Di Gioia D, Dresse M, Mayr D, Nagel D, Heinemann V, and Stieber P (2015). Serum HER2 in combination with CA 15-3 as a parameter for prognosis in patients with early breast cancer. *Clin Chim Acta* **440**, 16–22.

[18] Incoronato M, Mirabelli P, Catalano O, Aiello M, Parente C, Soricelli A, and Nicolai E (2014). CA15-3 is a useful serum tumor marker for diagnostic integration of hybrid positron emission tomography with integrated computed tomography during follow-up of breast cancer patients. *BMC Cancer* **14**, 356. http://dx.doi.org/10.1186/1471-2407-14-356.

[19] Grzywa R, Lupicka-Slowik A, Walczak M, Idzi M, Bobrek K, Boivin S, Gawel A, Stefaniak T, Oleksyszyn J, and Sienczyk M (2014). Highly sensitive detection of cancer antigen 15-3 using novel avian IgY antibodies. *ALTEX* **31**, 43–52.

[20] Curry JM, Thompson KJ, Rao SG, Besmer DM, Murphy AM, Grdzelishvili VZ, Ahrens WA, McKillop IH, Sindram D, and Iannitti DA, et al (2013). The use of a novel MUC1 antibody to identify cancer stem cells and circulating MUC1 in mice and patients with pancreatic cancer. *J Surg Oncol* **107**, 713–722.

[21] Chen D, Xia J, Tanaka Y, Chen H, Koido S, Wernet O, Mukherjee P, Gendler SJ, Kufe D, and Gong J (2003). Immunotherapy of spontaneous mammary carcinoma with fusions of dendritic cells and mucin 1-positive carcinoma cells. *Immunology* **109**, 300–307.

[22] Roy LD, Sahraei M, Subramani DB, Besmer D, Nath S, Tinder TL, Bajaj E, Shanmugam K, Lee YY, and Hwang SI, et al (2011). MUC1 enhances invasiveness of pancreatic cancer cells by inducing epithelial to mesenchymal transition. *Oncogene* **30**, 1449–1459.

[23] Nath S, Roy LD, Grover P, Rao S, and Mukherjee P (2015). Mucin 1 regulates Cox-2 gene in pancreatic cancer. *Pancreas* **44**, 909–917.

[24] Hardesty DA, Thind H, Zabramski JM, Spetzler RF, and Nakaji P (2014). Safety, efficacy, and cost of intraoperative indocyanine green angiography compared to intraoperative catheter angiography in cerebral aneurysm surgery. *J Clin Neurosci* **21**, 1377–1382.

[25] Rowse GJ, Ritland SR, and Gendler SJ (1998). Genetic modulation of neu proto-oncogene-induced mammary tumorigenesis. *Cancer Res* **58**, 2675–2679.

[26] Guy CT, Cardiff RD, and Muller WJ (1992). Induction of mammary tumors by expression of polyomavirus middle T oncogene: a transgenic mouse model for metastatic disease. *Mol Cell Biol* **12**, 954–961.

[27] Fluck MM and Schaffhausen BS (2009). Lessons in signaling and tumorigenesis from polyomavirus middle T antigen. *Microbiol Mol Biol Rev* **73**, 542–563.

[28] Perou CM, Sorlie T, Eisen MB, van de Rijn M, Jeffrey SS, Rees CA, Pollack JR, Ross DT, Johnsen H, and Akslen LA, et al (2000). Molecular portraits of human breast tumours. *Nature* **406**, 747–752.

[29] Sorlie T (2007). Molecular classification of breast tumors: toward improved diagnostics and treatments. *Methods Mol Biol* **360**, 91–114.

[30] Norum JH, Andersen K, and Sorlie T (2014). Lessons learned from the intrinsic subtypes of breast cancer in the quest for precision therapy. *Br J Surg* **101**, 925–938.

[31] Rutter CE, Yao X, Mancini BR, Aminawung JA, Chagpar AB, Saglam O, Hofstatter EW, Abu-Khalaf M, Gross CP, and Evans SB (2016). Influence of a 21-gene recurrence score assay on chemotherapy delivery in breast cancer. *Clin Breast Cancer* **16**, 59–62

[32] Stemmer SM, Klang SH, Ben-Baruch N, Geffen DB, Steiner M, Soussan-Gutman L, Merling S, Svedman C, Rizel S, and Lieberman N (2013). The impact of the 21-gene Recurrence Score assay on clinical decision-making in node-positive (up to 3 positive nodes) estrogen receptor–positive breast cancer patients. *Breast Cancer Res Treat* **140**, 83–92.

[33] Cobain EF and Hayes DF (2015). Indications for prognostic gene expression profiling in early breast cancer. *Curr Treat Options Oncol* **16**, 23. http://dx.doi.org/10.1007/s11864-015-0340-x.

[34] McVeigh TP, Hughes LM, Miller N, Sheehan M, Keane M, Sweeney KJ, and Kerin MJ (2014). The impact of Oncotype DX testing on breast cancer management and chemotherapy prescribing patterns in a tertiary referral centre. *Eur J Cancer* **50**, 2763–2770.

[35] Retsky M, Demicheli R, and Hrushesky W (2003). Breast cancer screening: controversies and future directions. *Curr Opin Obstet Gynecol* **15**, 1–8.

[36] Nicolini A, Carpi A, and Tarro G (2006). Biomolecular markers of breast cancer. *Front Biosci* **11**, 1818–1843.

[37] Stieber P, Nagel D, Blankenburg I, Heinemann V, Untch M, Bauerfeind I, and Di Gioia D (2015). Diagnostic efficacy of CA 15-3 and CEA in the early detection of metastatic breast cancer—a retrospective analysis of kinetics on 743 breast cancer patients. *Clin Chim Acta* **448**, 228–231.

[38] Debald M, Abramian A, Nemes L, Dobler M, Kaiser C, Keyver-Paik MD, Leutner C, Holler T, Braun M, and Kuhl C, et al (2015). Who may benefit from preoperative breast MRI? A single-center analysis of 1102 consecutive patients with primary breast cancer. *Breast Cancer Res Treat* **153**, 531–537.

[39] Goldenberg DM and Nabi HA (1999). Breast cancer imaging with radiolabeled antibodies. *Semin Nucl Med* **29**, 41–48.

[40] Sampath L, Kwon S, Ke S, Wang W, Schiff R, Mawad ME, and Sevick-Muraca EM (2007). Dual-labeled trastuzumab-based imaging agent for the detection of

human epidermal growth factor receptor 2 overexpression in breast cancer. *J Nucl Med* **48**, 1501–1510.

[41] Lutje S, Rijpkema M, Franssen GM, Fracasso G, Helfrich W, Eek A, Oyen WJ, Colombatti M, and Boerman OC (2014). Dual-modality image-guided surgery of prostate cancer with a radiolabeled fluorescent anti-PSMA monoclonal antibody. *J Nucl Med* **55**, 995–1001.

[42] Chatalic KL, Veldhoven-Zweistra J, Bolkestein M, Hoeben S, Koning GA, Boerman OC, de Jong M, and van Weerden WM (2015). A novel (1)(1)(1)In-labeled anti-prostate-specific membrane antigen nanobody for targeted SPECT/CT imaging of prostate cancer. *J Nucl Med* **56**, 1094–1099.

[43] Signore A, Capriotti G, Chianelli M, Bonanno E, Galli F, Catalano C, Quintero AM, De Toma G, Manfrini S, and Pozzilli P (2015). Detection of insulitis by pancreatic scintigraphy with 99mTc-labeled IL-2 and MRI in patients with LADA (Action LADA 10). *Diabetes Care* **38**, 652–658.

[44] Chetlen A, Mack J, and Chan T (2016). Breast cancer screening controversies: who, when, why, and how? *Clin Imaging* **40**, 279–282

[45] Rosso A, Lang K, Petersson IF, and Zackrisson S (2015). Factors affecting recall rate and false positive fraction in breast cancer screening with breast tomosynthesis—a statistical approach. *Breast* **24**, 680–686.

[46] Rhodes DJ, Radecki Breitkopf C, Ziegenfuss JY, Jenkins SM, and Vachon CM (2015). Awareness of breast density and its impact on breast cancer detection and risk. *J Clin Oncol* **33**, 1143–1150.

[47] Kemp Jacobsen K, O'Meara ES, Key D, D S M Buist D, Kerlikowske K, Vejborg I, Sprague BL, Lynge E, and von Euler-Chelpin M (2015). Comparing sensitivity and specificity of screening mammography in the United States and Denmark. *Int J Cancer* **137**, 2198–2207.

[48] Slanetz PJ, Freer PE, and Birdwell RL (2015). Breast-density legislation—practical considerations. *N Engl J Med* **372**, 593–595.